ADVANCED FUNCTIONAL MATERIALS
www.afm-journal.de

Overall Design of a Gradient-Ordered Membrane Electrode Assembly for Direct Liquid Fuel Cells

Zhefei Pan, Fengjia Xie, Zhewei Zhang, Zhen Zhao, Lizhen Wu, Wenzhi Li, Yao Zhu, Xiaoyu Huo, Yun Liu, Xuming Zhang, Rong Chen, and Liang An**

The direct liquid fuel cell (DLFC) constitutes a promising energy conversion system that directly conveys the chemical energy of liquid fuels into electrical energy. In certain DLFCs, gas is produced as a product of electrochemical reactions during operation. However, the accumulation of gas inside the porous electrode can significantly hinder the transport of reactants, leading to the failure of active sites and severe concentration loss. To address this issue, a gradient-ordered membrane electrode assembly (MEA) is designed and fabricated, consisting of a dual-gradient diffusion layer that comprises a pore-size gradient and a wettability gradient as well as a catalyst layer constructed by nanoneedle catalyst. This MEA promptly removes the produced gas and delivers the fresh solution, thereby enhancing the cell power output and stability. The fuel cell with the gradient-ordered MEA achieves a remarkable peak power density of 177 mW cm^{-2} and a discharging time of 19 h, which are more than four times and 30 times, respectively, higher than those of the conventional MEA.

1. Introduction

In recent decades, the world has experienced a substantial and ongoing increase in energy demand, accompanied by a growing emphasis on clean and sustainable energy sources.[1,2] Fuel cell systems have attracted significant interest in this context due to their high energy conversion efficiency and environmental benefits, presenting a promising solution to meet the rising energy demands while minimizing adverse environmental impact.[3,4] Fuel cell technology has witnessed remarkable advancements to date, leading to the development of various types of fuel cells to cater to different applications and requirements.[5] Among them, proton exchange membrane fuel cells (PEMFCs) fed by hydrogen have gained prominence as pioneering fuel cells with extensive applications, particularly in the automotive industry.[6] The utilization of hydrogen as a fuel holds immense potential for achieving clean energy goals.[7,8] However, challenges such as hydrogen production, transportation, and storage present significant hurdles that need to be addressed for safer and more cost-efficient solutions.[9]

As an alternative to the hydrogen-dependent fuel cells, direct liquid fuel cells (DLFCs) running on liquid fuels, such as methanol, ethanol, ammonia and formate, have come to the stage and captured global attention.[10–13] Unlike indirect fuel cells, DLFCs directly convert the chemical energy stored in liquid fuels into electrical energy without needing an external reforming process.[14,15] DLFCs exhibit carbon-neutral characteristics, utilize sustainable fuels, possess high energy density, and offer simple transportation, storage and handling.[16] However, certain challenges have arisen in developing DLFCs, including the high cost and loading of catalysts, generation of by-products, fuel safety concerns, and unproven long-term

Z. Pan, R. Chen
Key Laboratory of Low-Grade Energy Utilization Technologies and Systems (Chongqing University)
Ministry of Education
Chongqing 400030, China
E-mail: rchen@cqu.edu.cn

Z. Pan, R. Chen
Institute of Engineering Thermophysics
Chongqing University
Chongqing 400030, China

Z. Pan, Z. Zhang, Z. Zhao, L. Wu, W. Li, Y. Zhu, X. Huo, Y. Liu, L. An
Department of Mechanical Engineering
The Hong Kong Polytechnic University
Hung Hom, Kowloon, Hong Kong SAR 999077, China
E-mail: liang.an@polyu.edu.hk

F. Xie, X. Zhang
Department of Applied Physics
The Hong Kong Polytechnic University
Hung Hom, Kowloon, Hong Kong SAR 999077, China

L. An
Research Institute for Sports Science and Technology
The Hong Kong Polytechnic University
Hung Hom, Kowloon, Hong Kong SAR 999077, China

The ORCID identification number(s) for the author(s) of this article can be found under https://doi.org/10.1002/adfm.202404710

DOI: 10.1002/adfm.202404710

durability on the fuel cell operation.[17] Concerning cell performance, a prominent issue that severely limits the performance of some DLFCs with gas evolution as a product is the inefficient removal of gas products within the membrane electrode assembly (MEA).[18,19] During operation, the liquid fuel is transported into the channels of the flow field and then from the diffusion layer to the catalyst layer, where it undergoes an electrochemical reaction.[20] As a result of the electrochemical reactions, gaseous product is thus evolved at the catalyst layer and discharged from the catalyst layer to flow channels through the diffusion layer.[21] For instance, nitrogen gas is produced due to the oxidation of liquid ammonia, and carbon dioxide gas is produced due to the oxidation of methanol/ethanol/formate in DLFCs.[22,23] With the fuel cell discharging, gaseous products are continuously generated as the reaction proceeds, and with a conventional MEA configuration that is constructed by coating a dense catalyst layer onto commercial porous carbon substrate (carbon cloth or carbon paper), the produced gas gradually accumulates and forms gas bubbles within the MEA.[24,25] A large number of bubbles block the channels and pores and obstruct the transport of liquid reactants, thus leading to the failure of active sites and severe concentration loss.[26,27] As a consequence, the rates of electrochemical reactions are slowed down, and the cell performance including power output and stability is degraded.[28]

To address this issue, various MEA designs have been proposed. Chang et al. developed a gradient loading catalyst electrode with an in-plane gradient loading catalyst that is lower near the inlet and higher close to the outlet. The performance of the gradient loading catalyst electrode was enhanced by up to 19.8% compared with the uniform loading catalyst, especially under high current densities.[29] Gao et al. presented a semi-ordered catalyst layer structure design that significantly diminishes mass transport resistance while enhancing proton transport. It exhibited significantly improved MEA performance by 24% compared to the conventional planar catalyst layer.[30] Balakrishnan et al. designed and fabricated tailored gas diffusion layers with a pore-size gradient to enhance the high current density performance and water management behavior of a PEM fuel cell. It exhibited a 131% higher peak power output compared to the conventional diffusion layer.[31] In this work, a gradient-ordered MEA is designed and fabricated, consisting of a dual-gradient diffusion layer that comprises a pore-size gradient and a wettability gradient as well as a catalyst layer constructed by nanoneedle catalyst. This MEA serves to enhance the cell performance by facilitating rapid removal of generated gas and efficient delivery of fresh solution. The dual-gradient diffusion layer consists of three layers of carbon mat, enabling a pore-size gradient from small to large pores and a pore-wall wettability gradient from hydrophilic to superhydrophilic.[32] The effectiveness of the dual-gradient design in facilitating gas detachment and removal is verified via the visualization approach and the electrochemical cell performance. In addition, through cell-level characterization based on a direct ammonia fuel cell, the fuel cell with the dual-gradient diffusion layer exhibits significant improvements in the peak power density from 18 to 62 mW cm^{-2}, as well as in the discharging time from 2.5 to 19 h, comparing to the conventional diffusion layer (carbon cloth). Furthermore, a gradient-ordered MEA is fabricated using the electrodeposition method to directly grow Pd and Au nanoneedle catalyst onto the two dual-gradient diffusion layers to form catalyst layers and separated by an anion exchange membrane. By integrating the advantages of the nanoneedle catalyst layer and the dual-gradient diffusion layer, the gas removal capability of the gradient-ordered MEA is intensively enhanced. Subsequently, cell-level comparisons are made with conventional MEA in a format-hydrogen peroxide fuel cell, which suffers from gas blockage at both electrodes. The fuel cell with the gradient-ordered MEA achieves a remarkable peak power density of 177 mW cm^{-2} and a discharging time of 19 h, which are more than four times and 30 times, respectively, higher than those of the conventional MEA.

2. Results and Discussion

2.1. Dual-Gradient Diffusion Layer

The dual-gradient diffusion layer contains a pore-size distribution gradient and a pore-wall wettability gradient, achieved by adopting three layers of carbon mats, each with different properties.[33] As shown in **Figure 1a**, the first layer as the support layer for the catalyst has the smallest pore size (≈1.9 µm) and highest hydrophilicity (the gas contact angle of 171.5°, which is a superhydrophilic state). The middle layer serves as the mediating role that has the medium pore size (≈3.8 µm) and hydrophilicity (gas contact angle of 149.3°). The third layer attached to the flow field exhibits the largest pore size (≈22.2 µm) and lowest hydrophilicity (gas contact angle of 145.7°). The pore size is moderated by the concentration of polyacrylonitrile (PAN) in the precursor solution; the higher concentration of PAN leads to the larger pore size of the carbon mat.[34] Figure 1b further precisely demonstrates that the average pore sizes are 1.4, 3.2, and 7.1 µm of 11%, 14%, and 17% PAN concentrations, respectively. In addition, the porosities of these layers are similar (85% for 11% PAN, 89% for 14% PAN, and 90% for 17% PAN), making the pore size a more dominant parameter of the porous structure. Figure S1 (Supporting Information) shows that the initial states of three layers are all hydrophobic, whose water contact angles are 104°, 106°, and 110° for 11%, 14% and 17% PAN, respectively. For them to be able to deliver fuel solution efficiently, they are treated to be hydrophilic via oxygen plasma.[35] As a result, all the water contact angles change to 0°, indicating their hydrophilic nature.[36] During the treatment, the plasma power and duration are carefully controlled to realize the wettability gradient of three layers, which is verified by the gas contact angle.[37]

Using the gradient and conventional diffusion layers, the catalyst is sprayed onto them to build up the electrode. The morphology of the dual-gradient electrode and conventional electrode is characterized by scanning electron microscopy (SEM). Figure 1c demonstrates the pore structure of the carbon mat manufactured with 11% PAN, and Figure 1d displays the catalyst layer uniformly distributed on the carbon substrate. Figure 1e depicts the interface between the catalyst-coated area (the upper position) and the uncoated area (the lower position). Figure 1f shows the carbon fiber coated with the catalyst of the conventional carbon cloth. It can be observed that the pore size of carbon cloth is remarkably larger than that of carbon mat, leading to the catalyst on the carbon cloth more easily detaching from the carbon cloth.[38]

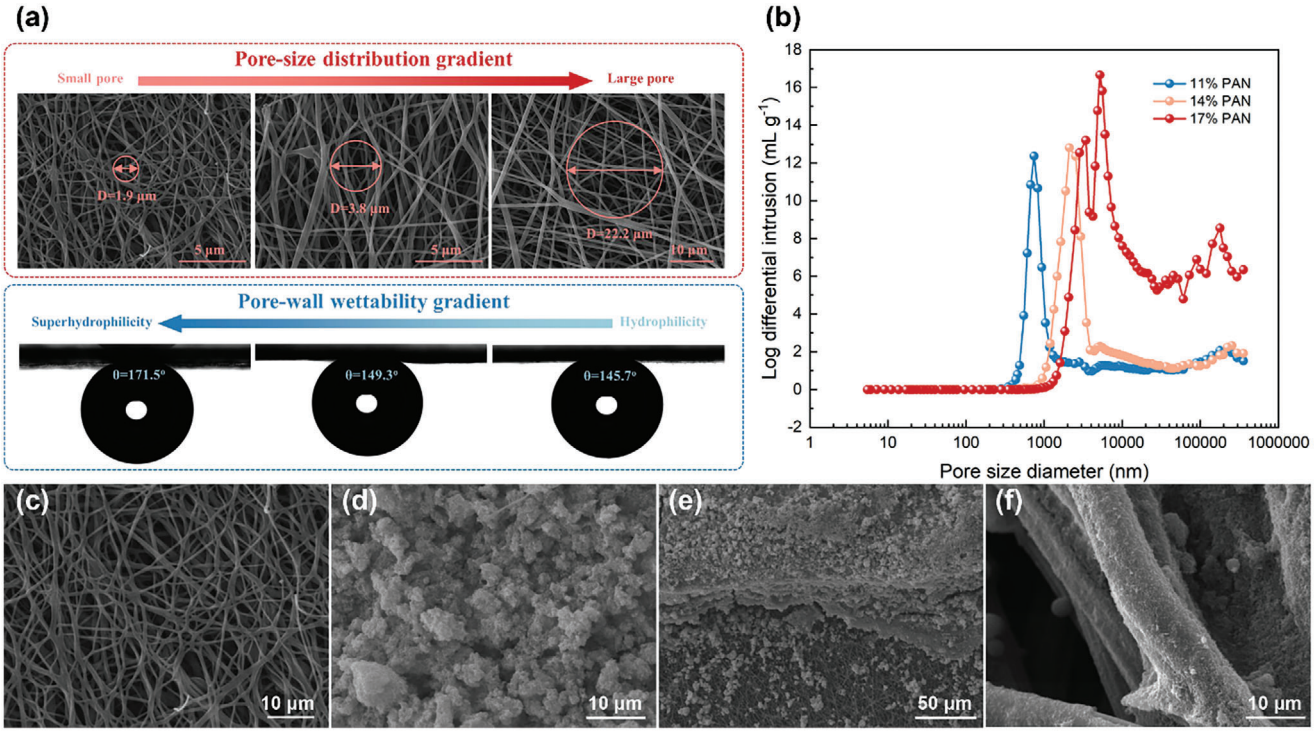

Figure 1. a) Pore-size gradient and pore-wall wettability gradient. b) Pore-size distribution of carbon mats with different PAN concentrations. Morphology of c) the dual-gradient diffusion layer, d) the catalyst layer on the dual-gradient diffusion layer, e) the edge of catalyst layer, and f) the carbon cloth-based electrode.

2.2. Visualization and Theoretical Analysis

To assess the impact of the dual-gradient diffusion layer on gas removal, a visualization test is conducted in the three-electrode system (**Figure** 2a and Video S1, Supporting Information). Both the dual-gradient electrode and conventional electrode with the same catalyst loading of 2.5 mg cm^{-2} PtRu/C are immersed in a solution containing 0.1 M ammonia and 3.0 M potassium hydroxide. A constant current of 100 mA cm^{-2} is applied at room temperature, resulting in nitrogen generation at the electrode through

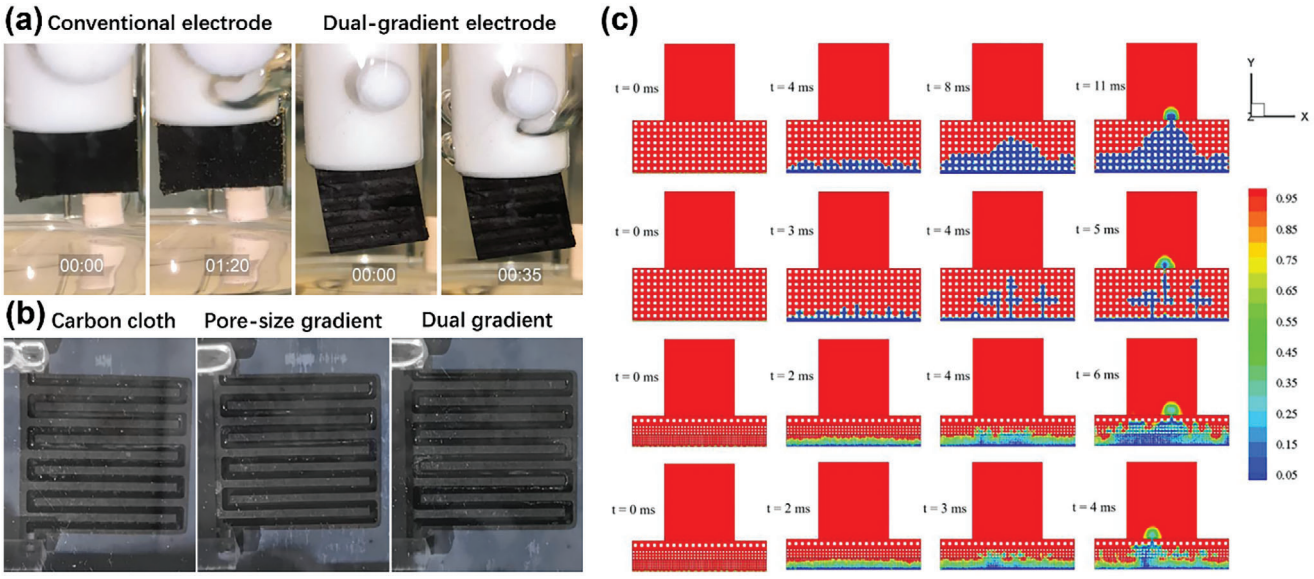

Figure 2. a) Bubble detachment time of dual-gradient electrode and conventional electrode in the three-electrode system. b) Two-phase flow patterns of electrodes with different diffusion layers in the flow cell. c) Theoretical analysis of the effect of diffusion layer design on gas removal ability.

the oxidation of ammonia. The nitrogen is initially saturated in the solution, then formed small bubbles attached to the electrode surface, gradually grows with time, and finally detached from the electrode due to the greater buoyancy.[39] The time duration from the appearance of the first bubble to its detachment from the electrode surface is analyzed to evaluate the gas-removal ability. For the conventional carbon cloth-based electrode, it takes 80 seconds for the first bubble to detach. In contrast, the bubble detachment time of the electrode with a dual-gradient diffusion layer significantly reduces to 36 s, saving more than half of the time. This indicates that the bubble detachment on the electrode surface is improved. Hence, the dual-gradient diffusion layer effectively facilitates the removal of gas products and the transport of liquid reactants.

The effect of diffusion layer gradient on gas removal from the electrode is also investigated at the cell-scale by collecting the removed gas and using the visualization method. Three types of electrodes, i.e., the conventional, single pore-size gradient, and dual-gradient electrodes, are assembled into a homemade cell. When the cell is operated at 90 °C, ammonia gas will evaporate from the ammonia solution and form a two-phase counter flow.[40] Ammonia can quickly dissolve into water, so saturated ammonia solution is used to accurately collect the produced ammonia gas. The collected solution is examined to determine the gas removal capability of the electrode. After a steady operation of 5 minutes, 9.0 mL of solution is collected using the conventional electrode, 12.0 mL of solution is collected using the pore-size gradient electrode, and 15.0 mL of solution is collected using the dual-gradient electrode. These results indicate that the pore-size gradient of the diffusion layer enhances gas removal and improves mass transport within the fuel cell, and the diffusion layer combining pore-size gradient and wettability gradient further enhances the gas removal ability. Afterwards, a visualization characterization is conducted between these three electrodes in terms of a two-phase flow pattern in the flow channels to verify the gas removal ability of different electrodes. During cell operation, gas produced on the catalyst layer diffuses through the diffusion layer into the flow channel, resulting in a two-phase flow in the flow channels Once the gas generated is difficult to remove from the electrode into flow channels, the ammonia oxidation reaction will be hindered, leading to less gas exiting in flow channels. In other words, since the fuel solution is fed at the same flow rate, it can be reasonably inferred that the electrode has a better gas removal ability when the flow channel has more gas. As the visualization results are shown in Figure 2b and Video S2 (Supporting Information), the cell with the conventional carbon cloth exhibits only half of the flow channels removing gas due to inadequate gas removal capability. In addition, the area is mainly downstream of the flow, indicating that the gas is not automatically pumped out. Otherwise, the gas can be found upstream of the flow because of the self-pumping ability of the electrode, even though the gas volume is not such large. In contrast, the cell with the pore-size gradient diffusion layer shows improved gas removal accounting for 75% of flow channels removing the gas, indicating a more favorable condition for fuel solution penetration. Notably, the cell with the dual-gradient diffusion layer displays that gas exits in all the flow channels, showcasing the superior gas removal capability of the designed electrode.[41] The gas removal ability between various designs is theoretically compared by the gas breakthrough time as an indicator. Here, breakthrough time refers to the time necessary to remove gas from the catalyst layer to the flow field channel; hence, a shorter breakthrough time indicating a quicker gas removal means that the electrode is less likely to be filled with gas. It is shown in Figure 2c that conventional design requires the longest breakthrough time of 11 ms and the introduction of a pore-size gradient or a wettability gradient beneficially shortens the breakthrough time to 6 and 5 ms, respectively, indicating an enhanced gas removal ability. Ultimately, the breakthrough time is further reduced to 4 ms with dual gradients, combining the advantages into one design. The movement of bubbles in porous media is caused by the capillary effect, which is essentially the combined effects of surface tension and wall adhesion in small pores. The pore size and surface wettability of porous media play a significant role in bubbles and water transport. The capillary pressure p_c is defined:[42]

$$p_c = p_g - p_w = \frac{4\sigma \cos\left(180° - \theta_g\right)}{d_{pore}} \quad (1)$$

where p_g and p_w are the gas and water pressures; d_{pore} and σ are the diameter of diffusion layer pore and the surface tension coefficient of water. θ_g is the gas contact angle. Along the through-plane direction (from catalyst layer to flow field), if with a fixed gas contact angle in the diffusion layer, as the pore diameter increases, the capillary pressure p_c decreases. Meanwhile, the $(180^\circ\text{-}\theta_g)$ increases, which means that $\cos(180^\circ\text{-}\theta_g)$ decreases. Therefore, p_c further decreases and bubbles will be removed faster (Figure S2, Supporting Information).

2.3. Cell Performance of Dual-Gradient Diffusion Layer

Cell-level performance tests are conducted to further investigate the impact of the diffusion layer on the performance of direct ammonia fuel cells using the mixture of ammonia and alkali as the fuel solution. The anode, utilizing a PtRu/C catalyst with a loading of 2.5 mg cm^{-2}, is supplied with a mixed solution of 3.0 M ammonia and 3.0 M potassium hydroxide at a rate of 2.0 mL min^{-1}. At the cathode using Pd/C catalyst with a loading of 0.5 mg cm^{-2}, pure oxygen is supplied at a flow rate of 10 sccm. As shown in **Figure 3a**, the fuel cell with the conventional carbon cloth exhibits a maximum current density of 150 mA cm^{-2} and a peak power density of 18 mW cm^{-2}. Furthermore, both the wettability-gradient diffusion layer and pore-size-gradient diffusion layer exhibit substantial improvements in cell performance. The cell with the wettability-gradient electrode achieves a maximum current density of 300 mA cm^{-2} and a peak power density of 39 mW cm^{-2}, slightly higher than the cell with the pore-size-gradient electrode, which achieves 250 mA cm^{-2} and 38 mW cm^{-2}, respectively. Figure S3 (Supporting Information) depicts that the carbon mats with uniform pore size and wettability could slightly improve the cell performance, and the introduction of the pore-size gradient and wettability gradient could significantly boost the cell performance. Impressively, the electrode with the dual-gradient diffusion layer demonstrates a significant enhancement in performance compared to other configurations. It achieves a maximum current density of 375 mA cm^{-2}, four times higher than

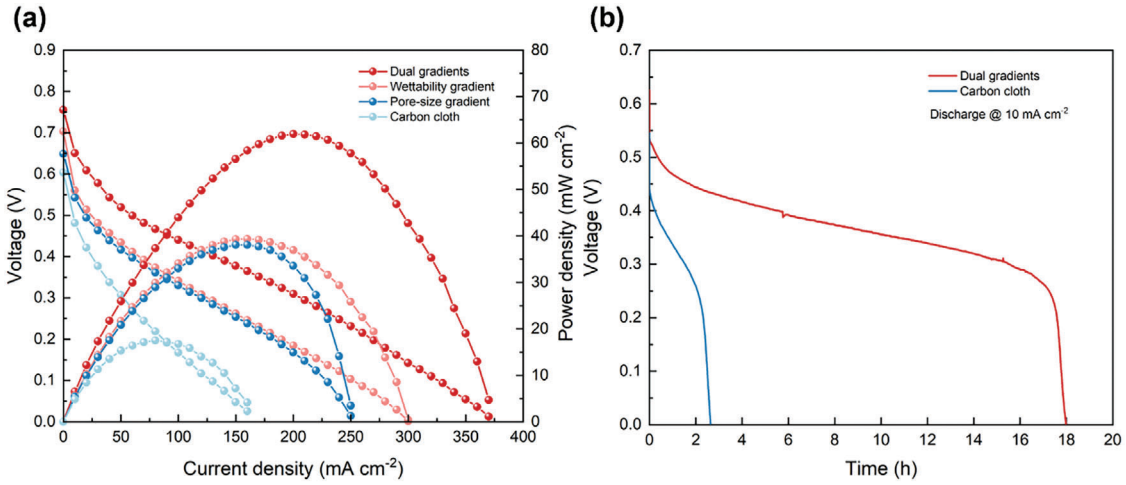

Figure 3. a) Polarization and power density curves of the fuel cell using different diffusion layers. b) Constant-current discharging behavior of the fuel cell using dual-gradient diffusion layer and carbon cloth.

the conventional one, and a peak power density of 62 mW cm^{-2}, more than three times that of the conventional configuration. These results highlight the significant performance enhancement of the DLFC, particularly the ammonia fuel cell, through effective gas bubble removal using the dual-gradient diffusion layer. The discharging performance of the direct ammonia fuel cell with the dual-gradient electrode is compared to that of the cell with the conventional electrode, as shown in Figure 3b. At a constant discharging current density of 10 mA cm^{-2}, the cell with the conventional electrode achieves a maximum discharging time of 2.5 h while the cell with the dual-gradient electrode demonstrates a remarkable improvement, with a maximum discharging time of 18 h, which is more than seven times longer. Furthermore, the voltage of the cell with the conventional electrode exhibits a rapid drop as the discharging proceeds. In contrast, the cell with the dual-gradient electrode displays a slower decrease in voltage over time, indicating a more stable discharging condition.[43] These results provide further evidence of the significant enhancement achieved by the dual-gradient diffusion layer in the performance of DLFCs.

2.4. Gradient-Ordered MEA

As gas is generated in the catalyst layer, gas removal from the catalyst layer is equally important. The gas is easily accumulated in the conventional particle-packed catalyst layer and blocks the porous structure.[44] Hence, the catalyst layers constructed by nanoneedle catalysts (Pd for formate oxidation on the anode and Au for hydrogen peroxide reduction on the cathode) are revolutionarily designed and fabricated. **Figure 4** shows the SEM images, X-ray diffraction (XRD) patterns, and transmission electron microscopy (TEM) images of Pd and Au catalyst layers. It can be seen from SEM images that both the Pd (Figure 4a) and Au (Figure 4d) catalysts grow in the form of needle-shaped structures. The Pd catalyst exhibits small arrow-shaped thorns, while

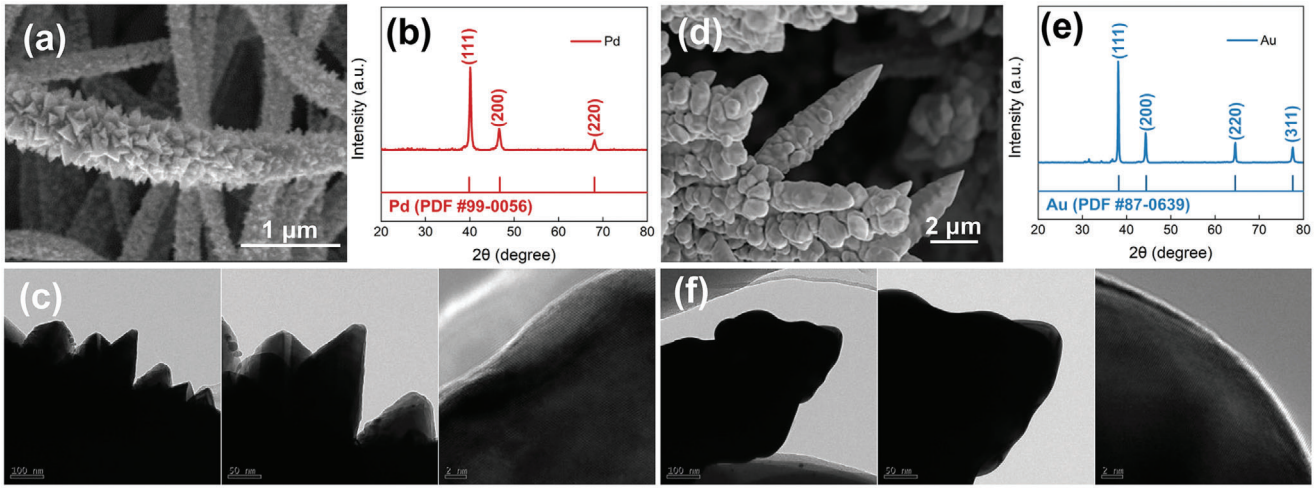

Figure 4. a) SEM image of Pd nanoneedle. b) XRD pattern of Pd nanoneedle. c) TEM images of Pd nanoneedle. d) SEM image of Au nanoneedle. e) XRD pattern of Au nanoneedle. f) TEM images of Au nanoneedle.

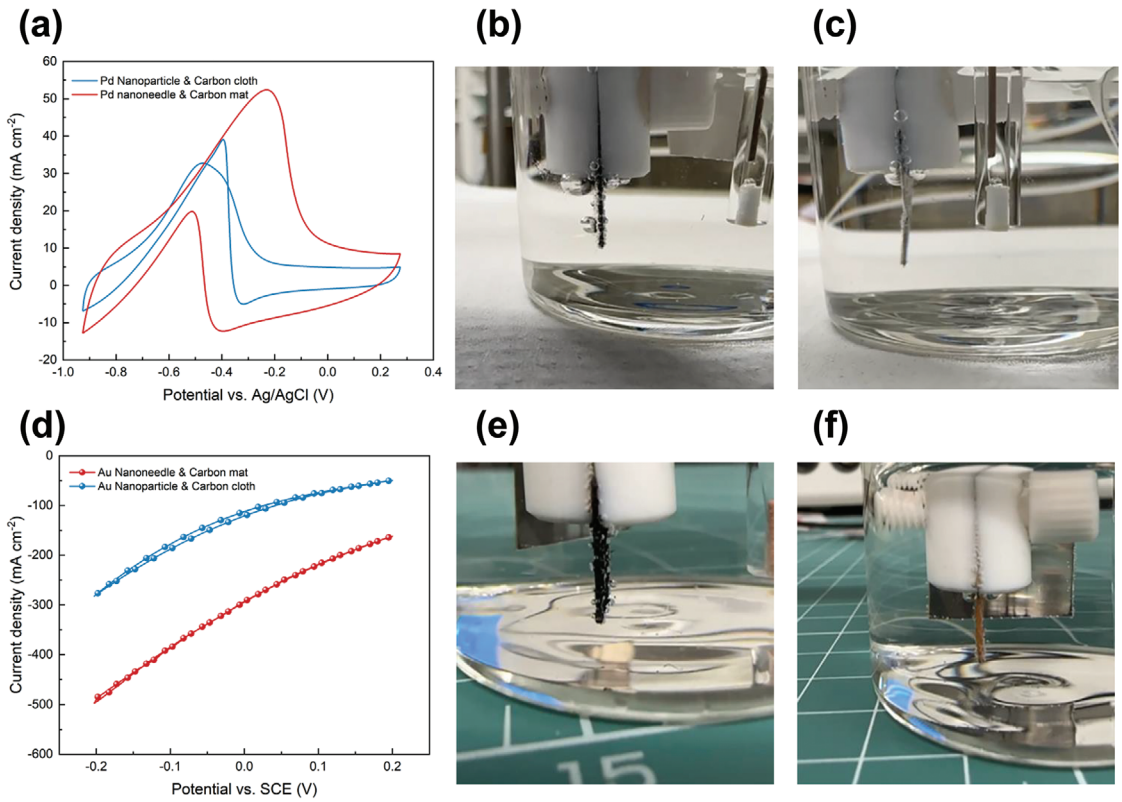

Figure 5. a) CV results of different electrodes in 0.1 M sodium formate and 1.0 M sodium hydroxide solution. b) Bubble behavior of conventional Pd electrode. c) Bubble behavior of Pd nanoneedle electrode. d) CV results of different electrodes in 4.0 M hydrogen peroxide and 0.05 M sulfuric acid solution. e) Bubble behavior of conventional Au electrode. f) Bubble behavior of Au nanoneedle electrode.

the Au catalyst displays a clustered shape with a thin end. The XRD results of Pd (Figure 4b) reveal that primary diffraction peaks detected for the (111), (200), and (220) facets occur at angles of 40.2°, 46.8°, and 68.3°, respectively, which are consistent with typical peaks of Pd (PDF#87-0639). In addition, the XRD results of Au (Figure 4e) reveal that primary diffraction peaks detected for the (111), (200), (220), and (311) facets occur at angles of 38.2°, 44.4°, 64.6° and 77.6°, respectively, which are consistent with typical peaks of Au (PDF#99-0056). TEM images (Figure 4a,f) further confirm the needle shape of catalysts and the dominant (111) facet of both Pd and Au, with an interlayer spacing of 0.224 and 0.235 nm, respectively, consistent with the XRD patterns. The needle-like morphology of catalysts could facilitate the rapid removal of gas generated at the catalyst surface.[45] Furthermore, the catalysts are evenly distributed on the fibers of the carbon mat, forming a porous architecture. This porous structure enables efficient mass transport through the interconnected pores and channels, which is crucial for initiating electrochemical reactions.

2.5. Visualization Characterization

Figure 5a presents the cyclic voltammetry (CV) results of the conventional electrode and Pd nanoneedle-based electrode, respectively. The conventional Pd electrode has a loading of 1.0 mg cm^{-2} while the Pd nanoneedle electrode has a loading as low as 0.34 mg cm^{-2}. Notably, the nanoneedle electrode with a lower catalyst loading exhibits a significantly higher current density compared to the conventional electrode at the same applied potential, indicating a superior electrochemical reaction rate. It is shown in Figure S4 (Supporting Information) that the nanoneedle structure constructed by electrodeposition exhibits superior catalytic activity than the nanoparticle structure formed by random packing, which is attributed to that more active sites of nanoneedle structure are exposed than the nanoparticle structure. To further validate their gas removal ability, a visualization test is conducted in the three-electrode system. For the anode, the electrode is immersed in a mixed solution of 0.1 M sodium formate and 1.0 M sodium hydroxide at room temperature, and a current of 50 mA is applied. Figure 5b,c and Video S3 (Supporting Information) show the bubble behavior of conventional electrode and nanoneedle electrode, respectively. It is noteworthy that the conventional electrode has larger bubbles evolved due to formate oxidation, and many bubbles are firmly attached to its surface. Even worse, bubbles grow and emerge into huge bubbles with time. All the bubble behaviors imply that the conventional electrode possesses a poor gas removal ability, and thus the active sites are covered by gas and not accessible by solution, degrading the electrochemical performance.[46] Whereas the nanoneedle electrode exhibits that the evolved bubbles are much smaller and effectively detached from the electrode. For the cathode, the electrode is immersed in a solution of 4.0 M hydrogen peroxide and 0.05 M sulfuric acid at room temperature for the CV test. The conventional Au electrode has a loading of 2.7 mg cm^{-2} while the Au

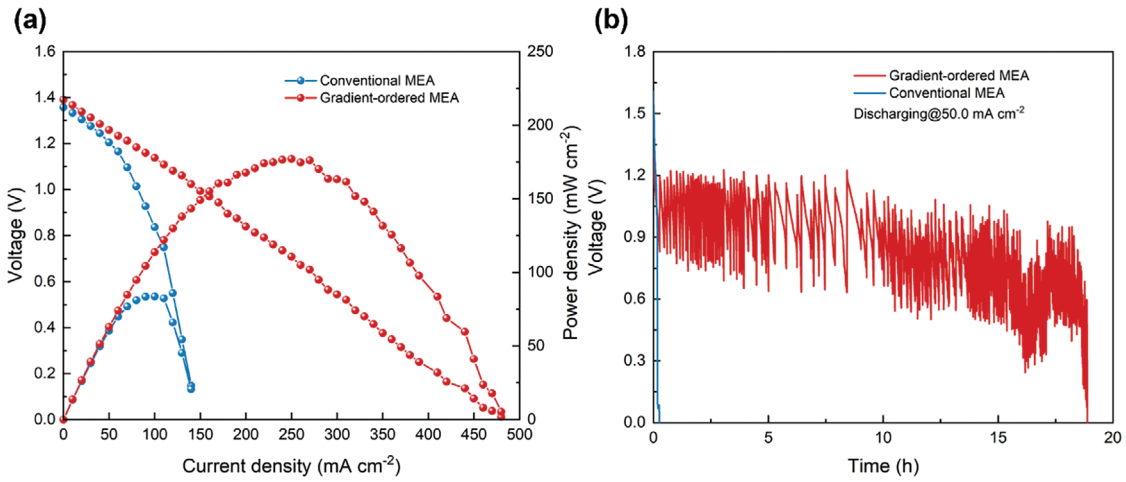

Figure 6. a) Polarization and power density curves of the fuel cell using different MEAs. b) Constant-current discharging behavior of the fuel cell using different MEAs.

nanoneedle electrode has a loading as low as 0.3 mg cm^{-2}. Impressively, the nanoneedle electrode with a lower catalyst loading yields a significantly higher current density, indicating its superior electrochemical performance (Figure 5d). Figure S5 (Supporting Information) shows that the nanoneedle catalyst has a lower Tafel slope of 25.34 mV dec^{-1}, indicating its superior electrocatalytic performance, because a smaller overpotential is required to reach a higher current density. In the visualization characterization (Figure 5e,f and Video S3, Supporting Information), hydrogen peroxide is not added because it is intensively decomposed to generate a large number of oxygen bubbles, which affects the observation of bubble behaviors.[47] Hence, only 0.05 M sulfuric acid solution is used and a current of 10 mA is applied for 30 seconds, such that the hydrogen evolution reaction is the demonstration reaction. A similar phenomenon can be observed that the conventional electrode has many bubbles firmly attached to its surface, and bubbles grow and emerge into huge bubbles with time. Whereas the nanoneedle electrode exhibits that the evolved bubbles are much smaller and effectively detached from the electrode. These outcomes provide further evidence confirming the superior gas removal performance of the nanoneedle catalyst layer.

2.6. Cell Performance of Gradient-Ordered MEA

Using the dual-gradient diffusion layer as the substrate for the nanoneedle catalyst layer, the gradient-ordered electrode is constructed (Figure S6, Supporting Information). MEA is overall redesigned by integrating the gradient-ordered electrodes as the anode and cathode, separated by an ion exchange membrane. To demonstrate the superiority of ordered MEA, the formate-hydrogen peroxide fuel cell is fabricated using the mixture of formate and alkali as the fuel solution, as this fuel cell may suffer from gas accumulation both in the anode and cathode. The treated Nafion 211 is employed as the cation exchange membrane. The operating temperature is maintained at 80 °C, and during operation, a mixture of 1.0 M formate and 2.0 M sodium hydroxide is supplied to the anode, while a solution of 4.0 M hydrogen peroxide and 1.0 M sulfuric acid is supplied to the cathode. **Figure** 6a illustrates the comparison of the cell performances between the conventional and ordered MEA. The conventional MEA demonstrates a maximum current density of 140 mA cm^{-2} with a peak power density of 84 mW cm^{-2}, whereas the ordered MEA exhibits a significant improvement, with a maximum current density of 480 mA cm^{-2} and a peak power density of 177 mW cm^{-2}. It achieves a maximum current three times higher than that of the conventional one and a peak power density more than two times higher. These enhancements can be attributed to the effective removal of gas bubbles from the electrode. Figure S7 (Supporting Information) summarizes the internal resistance of different electrodes. It is found that the internal resistance of carbon cloth and carbon mat with pore-size regulation is similar, while the internal resistance increases with wettability regulation. This is attributed to the O2 plasma treatment may reduce the electron conductivity of carbon mats. Although the diffusion layer with dual gradients has the highest internal resistance, it still outputs the best power density, which indicates the positive effect of efficient gas removal outweighs the negative effect of increased ohmic loss. It can be seen from Figure S8 (Supporting Information) that at the high-frequency region, the gradient-ordered MEA has a lower resistance than the conventional MEA, which is consistent with the results of internal resistance in Figure S7 (Supporting Information), and at the low-frequency region, the gradient-ordered MEA still exhibits a better mass transfer, which can be ascribed to the efficient gas removal. The discharging performance is also evaluated to assess the operating stability of the fuel cells (Figure 6b). Under a constant discharging current of 50.0 mA cm^{-2}, the conventional MEA only discharges for less than 0.5 h (Figure S9, Supporting Information), whereas the fuel cell equipped with ordered MEA achieves an impressive maximum discharging time of 19 hours. During the discharging process, the voltage of the conventional cell abruptly drops from 1.6 V to around 0.1 V within the first hour, and then decreases to 0. In contrast, the cell with ordered MEA experiences a gradual voltage decrease from 1.3 V. It exhibits fluctuations around 1.0 V for nearly 19 h before eventually dropping to 0. These voltage fluctuations can be attributed to

the gas removal process.[9] The generated gas bubbles at both anode and cathode may be attached to the catalyst surface to cover the active sites, and accumulate in the porous electrode to block the reactant supply. Once the gas bubbles are swept out from the cell, the active sites will be exposed and delivery channels will be unchoked again, both of which are beneficial for maintaining a higher cell voltage.[48]

3. Conclusion

In this work, a gradient-ordered MEA is designed and fabricated, consisting of a dual-gradient diffusion layer comprising a pore-size gradient and a wettability gradient as well as a catalyst layer constructed by nanoneedle catalyst. Through comprehensive characterizations and visualization tests, the gradient-ordered MEA serves to enhance the cell performance by facilitating rapid removal of generated gas and efficient delivery of fresh solution. The direct ammonia fuel cell with the dual-gradient diffusion layer exhibits significant improvements in the peak power density from 18 to 62 mW cm^{-2}, as well as in the discharging time from 2.5 to 19 h, compared to the conventional diffusion layer. Furthermore, the formate-hydrogen peroxide fuel cell with the gradient-ordered MEA achieves a remarkable peak power density of 175 mW cm^{-2} and a discharging time of 19 hours, which are more than four times and thirty times, respectively, higher than those of the conventional MEA. The huge improvement is attributed to the combination of advantages of the dual-gradient diffusion layer and nanoneedle catalyst layer, both of which intensively enhance the gas removal capability of the gradient-ordered MEA. In summary, this work presents a novel approach to improve the performance of DLFCs by designing and fabricating a novel MEA with enhanced gas removal and solution supply, providing promising insights into improving DLFC efficiency and advancing clean energy conversion technologies.

Supporting Information

Supporting Information is available from the Wiley Online Library or from the author.

Acknowledgements

Z.P. and F.X. contributed equally to this work. The work described in this paper was supported by a grant from the National Natural Science Foundation of China (52161160333), a grant from the Research Grants Council of the Hong Kong Special Administrative Region, China (N_PolyU559/21) and a grant from the Research Institute for Sports Science and Technology at The Hong Kong Polytechnic University (CD5L).

Conflict of Interest

The authors declare no conflict of interest.

Data Availability Statement

The data that support the findings of this study are available from the corresponding author upon reasonable request.

Keywords

direct liquid fuel cells, dual-gradient diffusion layer, gas removal, membrane electrode assembly, nanoneedle catalyst layer

Received: March 18, 2024
Revised: May 3, 2024
Published online: June 5, 2024

[1] Z. Liu, Z. Deng, G. He, H. Wang, X. Zhang, J. Lin, Y. Qi, X. Liang, *Nat. Rev. Earth Environ.* **2022**, *3*, 141.
[2] X. Shi, O. C. Esan, X. Huo, Y. Ma, Z. Pan, L. An, T. S. Zhao, *Prog. Energy Combust. Sci.* **2021**, *85*, 100926.
[3] Z. F. Pan, L. An, T. S. Zhao, Z. K. Tang, *Prog. Energy Combust. Sci.* **2018**, *66*, 141.
[4] O. C. Esan, X. Shi, Z. Pan, X. Huo, L. An, T. S. Zhao, *Adv. Energy Mater.* **2020**, *10*, 2000758.
[5] K. Jiao, J. Xuan, Q. Du, Z. Bao, B. Xie, B. Wang, Y. Zhao, L. Fan, H. Wang, Z. Hou, S. Huo, N. P. Brandon, Y. Yin, M. D. Guiver, *Nature* **2021**, *595*, 361.
[6] F. Xiao, Q. Wang, G.-L. Xu, X. Qin, I. Hwang, C.-J. Sun, M. Liu, W. Hua, H.-w. Wu, S. Zhu, J.-C. Li, J.-G. Wang, Y. Zhu, D. Wu, Z. Wei, M. Gu, K. Amine, M. Shao, *Nat. Catal.* **2022**, *5*, 503.
[7] Z. F. Pan, L. An, C. Y. Wen, *Appl. Energy* **2019**, *240*, 473.
[8] X. Shi, X. Huo, O. C. Esan, Z. Pan, L. Yun, L. An, T. S. Zhao, *Energy AI* **2023**, *14*, 100275.
[9] Z. Pan, Z. Zhang, W. Li, X. Huo, Y. Liu, O. C. Esan, Q. Wu, L. An, *ACS Energy Lett.* **2023**, *8*, 3742.
[10] T. S. Zhao, C. Xu, R. Chen, W. W. Yang, *Prog. Energy Combust. Sci.* **2009**, *35*, 275.
[11] L. An, T. S. Zhao, Y. S. Li, *Renewable Sustainable Energy Rev.* **2015**, *50*, 1462.
[12] Z. Pan, Y. Liu, A. Tahir, O. Christopher Esan, J. Zhu, R. Chen, L. An, *Appl. Energy* **2022**, *322*, 119463.
[13] Z. Pan, Y. Liu, Z. Zhang, Z. Zhao, J. Zhu, R. Chen, L. An, *Int. J. Hydrogen Energy* **2022**, *47*, 38361.
[14] G. Jeerh, M. Zhang, S. Tao, *J. Mater. Chem. A* **2021**, *9*, 727.
[15] X. Shi, Y. Dai, O. C. Esan, X. Huo, L. An, T. Zhao, *ACS Appl. Mater. Interfaces* **2021**, *13*, 48795.
[16] S. Park, J. M. Vohs, R. J. Gorte, *Nature* **2000**, *404*, 265.
[17] S. Giddey, S. P. S. Badwal, A. Kulkarni, C. Munnings, *Prog. Energy Combust. Sci.* **2012**, *38*, 360.
[18] H. Yang, T. S. Zhao, Q. Ye, *J. Power Sources* **2005**, *139*, 79.
[19] M. Tanveer, T. Ambreen, H. Khan, G. Man Kim, C. Woo Park, *Energy Convers. Manage.* **2022**, *264*, 115732.
[20] Z. Pan, B. Huang, L. An, *Int. J. Energy Res.* **2019**, *43*, 2583.
[21] Z. Pan, Y. Bi, L. An, *Appl. Therm. Eng.* **2019**, *147*, 1115.
[22] Y. Liu, Z. Pan, O. C. Esan, X. Xu, L. An, *Energy Fuels* **2022**, *36*, 13203.
[23] X. Su, Z. Pan, L. An, Y. Yu, *Int. J. Heat Mass Transfer* **2021**, *164*, 120629.
[24] L. Wan, Z. Xu, Q. Xu, P. Wang, B. Wang, *Energy Environ. Sci.* **2022**, *15*, 1882.
[25] X. Shi, X. Huo, O. C. Esan, Y. Dai, L. An, T. S. Zhao, *ACS Appl. Mater. Interfaces* **2022**, *14*, 18600.
[26] S. Jung, Y. Leng, C.-Y. Wang, *Electrochim. Acta* **2014**, *134*, 35.
[27] X. Shi, X. Huo, O. C. Esan, Y. Ma, L. An, T. S. Zhao, *J. Power Sources* **2021**, *506*, 230198.
[28] A. Lindermeir, G. Rosenthal, U. Kunz, U. Hoffmann, *J. Power Sources* **2004**, *129*, 180.
[29] Z. Chang, J. Zhang, W. Zhang, H. Su, L. Xing, Q. Ma, H. Zhang, Q. Xu, *Processes* **2021**, *9*, 1787.

[30] J. Gao, H. Wang, Z. Zhang, Y. Chen, D. Li, M. Zhou, M. Chai, Y. Li, *J. Power Sources* **2024**, *606*, 234516.
[31] M. Balakrishnan, P. Shrestha, N. Ge, C. Lee, K. F. Fahy, R. Zeis, V. P. Schulz, B. D. Hatton, A. Bazylak, *ACS Appl. Energy Mater.* **2020**, *3*, 2695.
[32] B. K. Kim, M. J. Kim, J. J. Kim, *ACS Appl. Mater. Interfaces* **2021**, *13*, 11940.
[33] C. Liu, X. Yan, F. Hu, G. Gao, G. Wu, X. Yang, *Adv. Mater.* **2018**, *30*, 1705713.
[34] X. Zhang, Y. Huang, X. Zhou, F. Wang, Z. Luo, Q. Wu, *J. Power Sources* **2020**, *448*, 227410.
[35] Y. Huang, Q. Yu, M. Li, S. Jin, J. Fan, L. Zhao, Z. Yao, *Chem. Eng. J.* **2021**, *418*, 129474.
[36] Z. Pan, Y. Bi, L. An, *Appl. Energy* **2020**, *258*, 114060.
[37] I. U. Chowdhury, P. Sinha Mahapatra, A. K. Sen, *Phys. Fluids* **2019**, *31*, 042111.
[38] F. Lapicque, M. Belhadj, C. Bonnet, J. Pauchet, Y. Thomas, *J. Power Sources* **2016**, *336*, 40.
[39] T. Kou, S. Wang, R. Shi, T. Zhang, S. Chiovoloni, J. Q. Lu, W. Chen, M. A. Worsley, B. C. Wood, S. E. Baker, E. B. Duoss, R. Wu, C. Zhu, Y. Li, *Adv. Energy Mater.* **2020**, *10*, 2002955.
[40] Y. Liu, Z. Pan, O. C. Esan, X. Huo, X. Shi, L. An, *J. Power Sources* **2023**, *570*, 233057.
[41] W. Wang, Z. Xie, K. Li, S. Yu, L. Ding, F.-Y. Zhang, *Curr. Opin. Electrochem.* **2022**, *35*, 101088.
[42] K. Jiao, X. Li, *Prog. Energy Combust. Sci.* **2011**, *37*, 221.
[43] Z. Pan, Y. Bi, L. An, *Appl. Energy* **2019**, *250*, 846.
[44] N. Trogisch, M. Koch, E. N. El Sawy, H. A. El-Sayed, *ACS Catal.* **2022**, *12*, 13715.
[45] Y. Zhou, Y. Yang, X. Zhu, T. Zhang, D.-d. Ye, R. Chen, Q. Liao, *Adv. Funct. Mater.* **2022**, *32*, 2201872.
[46] Z. Pan, Z. Zhang, A. Tahir, O. C. Esan, X. Liu, H. Wang, L. An, *Int. J. Energy Res.* **2022**, *46*, 13820.
[47] J. Qiu, W. Tang, B. Bao, S. Zhao, *Chem. Eng. J.* **2021**, *424*, 130486.
[48] M. S. Alias, S. K. Kamarudin, A. M. Zainoodin, M. S. Masdar, *Int. J. Hydrogen Energy* **2020**, *45*, 19620.